P4.9 MESOSCALE DISTRIBUTION OF SPECTRAL ACTINIC FLUX AND PHOTOLYSIS IN CONDITIONS OF VARIABLE CLOUD COVER AND HIGH SURFACE ALBEDO

Melanie A. Wetzel*, William R. Stockwell, Dong Chul Kim and Christopher Loughner
Desert Research Institute, Reno, Nevada

1. INTRODUCTION

Exposure to ultraviolet (UV) radiation has serious impacts on living organisms from microbes to humans (Frederick and Lubin, 1988; Madronich, 1992). Most damaging are rays in the UVB (280-320 nm) wavelength region which have been linked to skin cancer (Williams and Green, 1996) as well as impairment of plant growth (Caldwell *et al*., 1998). Cloud cover, solar zenith angle and ozone column amount normally provide the largest degree of fluctuation in UV irradiance at the surface, and both are subject to regional and global atmospheric process trends. Depletion of stratospheric ozone as well as alterations in cloud climatology can cause significant impacts on UV irradiance (Herman *et al.,* 1999) and tropospheric chemistry (Madronich and Granier, 1992).

Use of satellite-obtained high resolution imagery offers an opportunity to monitor more precisely the spatial and temporal distribution of cloud over a location. Meerkotter *et al.* (1997) used the NOAA Advanced Very High Resolution Radiometer (AVHRR) with addition of global ozone data for a case study of high-resolution surface UV mapping. Verdebout (2000) has used geostationary Meteosat and ancillary data over Europe to produce time series maps of surface UV radiation at 0.05^{o} resolution. Geostationary satellite data have the advantage of high temporal resolution and thus can be used to more accurately estimate total daily UV exposure and time-integrated photochemical reaction processes.

In this study, we demonstrate a procedure for using GOES data with surface measurements and radiative transfer modeling to map the mesoscale distribution of spectral UV radiation over a mountainous region in Colorado.

2. GROUND-BASED MEASUREMENTS

Ground-based measurements were utilized for comparisons to model-derived spectral irradiances as well as for evaluation of the satellite-derived estimates of irradiance from the satellite datasets. The USDA UVB Monitoring and Research Network (Bigelow *et al.,* 1998) consists of 28 US and Canadian sites and one New Zealand site which measure total horizontal, direct, and diffuse UV irradiances with a Yankee Environmental Systems (YES) ultraviolet shadow-band radiometer (UV-MFRSR) at seven nominal UV wavelengths: 300, 305, 311, 317, 325, 332, and 368 nm with a full-width at half maximum of about 2.0 nm. The irradiance data are also used to retrieve spectral optical depth and ozone column amount (Gao *et al.,* 2001).

Additional parameters are operationally measured at the UVB Network sites including visible and near-infrared spectral irradiances using a YES Vis-MFRSR (Harrison and Michalsky, 1994) instrument, broadband UV-B irradiance, air temperature, relative humidity, barometric pressure, and upwelling shortwave radiation. This study utilized data from the Desert Research Institute's (DRI) Storm Peak Laboratory near Steamboat Springs, Colorado and other UVB Network sites in the surrounding region. Measurements at the Storm Peak Laboratory (SPL) also included spectral actinic flux across the UV and visible range, using upward- and downward-looking spectroradiometers.

3. RETRIEVAL OF UV SPECTRAL PARAMETERS

A schematic diagram in Figure 1 illustrates the procedure for retrieval of UV spectral irradiance. Radiative transfer modeling is carried out to prepare arrays for a range of direct and diffuse irradiances under varying conditions of surface albedo and cloud optical depth. Spectral irradiances for clear and cloudy scenes were calculated using the Santa Barbara DISORT Atmospheric Radiative Transfer (SBDART) model (Ricchiazzi *et al*., 1998). The code was modified to use the extraterrestrial solar flux obtained by the SUSIM spectrometer aboard the Space Shuttle Atlas 3 flight (data corrected from vacuum to air). The accuracy of this spectrum was recently validated by Gröbner and Kerr (2001). Ozone absorption cross-sections were based on the work of Molina and Molina (1986) as used in LOWTRAN (Kneizys *et al*., 1983). Model input for ozone column amount was obtained from NASA TOMS database and the USDA UV-MFRSR database.

The SBDART model default values for aerosol vertical profile in high-visibility conditions and background stratospheric loading were applied, and time-specific

*Corresponding author address:
Dr. Melanie A. Wetzel, Division of Atmospheric Sciences, Desert Research Institute, 2215 Raggio Parkway, Reno NV 89512-1095 ;
email: wetzel@dri.edu

values of spectral aerosol optical depth obtained from USDA UVB site instrumentation were used for case study validation when available. Spectral irradiance, ozone and optical depth parameters derived from the site measurement data are valuable both as input to the radiative transfer calculations for the locale, and for assessing the sensitivity of retrieval methods to use of operational satellite remote sensing products as input data.

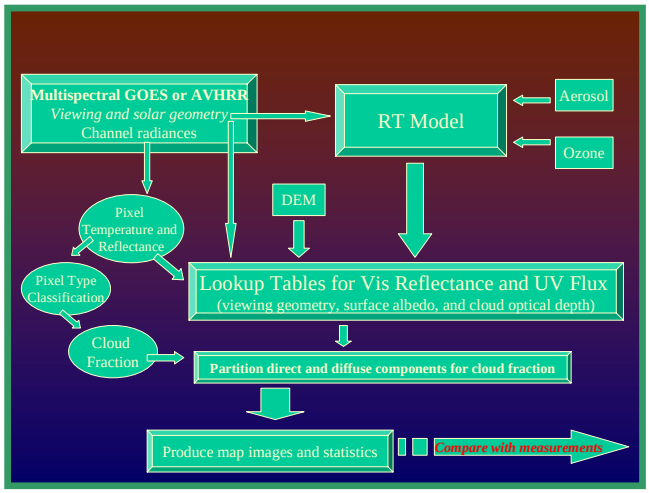

Figure 1. Schematic diagram for the production of mesoscale mapped distributions of spectral downwelling UV irradiance using GOES (or AVHRR) data with radiative transfer modeling.

The retrieval procedure for the mesoscale distribution of UV irradiances uses satellite image data in the visible (0.55 μm), near infrared (3.9 μ m) and thermal infrared (11 μm) bands. GOES pixel resolution is 1 km in the visible channel and 4 km in the infrared channels used. The satellite data were remapped from pixels to a gridded area centered on a measurement site. All cells within the study region were assigned a scene type based on multispectral analysis of the image data. The channel threshold technique is similar to the classification method of Turner *et al*. (2001). Gridded cell values of the visible reflectance were scaled by the solar zenith angle (SZA).

Reflectance threshold values were used for discrimination of land from snow or cloud. Cells were classified as (non-snow) land surfaces if visible reflectance is less than specified threshold value. Reflectance in the near infrared (NIR) was obtained by subtracting the emitted thermal component (obtained from the radiative-equivalent temperature determined from the thermal channel image data) and then scaling the reflected radiance by the SZA. Cells that passed the visible reflectance test were further classified as snow or cloud by the use of NIR threshold and thermal threshold tests. Snow and ice cloud have a low value of NIR reflectance. Snow is discriminated from ice cloud by NIR reflectance plus thermal infrared (TIR) threshold tests. Clouds are either very bright in the NIR (if composed primarily of water droplets), or quite cold in the TIR (high ice clouds).

Grid cell types determined from the classification procedure were used to assign model-derived radiative flux components at each point. Cloud optical depth was estimated by interpolation from visible reflectance for those pixels classified as cloudy. The value of cloud optical depth for each cloudy grid cell was obtained by interpolation from arrays of model results for variable surface albedo (model input values beginning at 0.05 and increasing in intervals of 0.10), cloud optical depth (model values increasing from 5 to 200), and sun-satellite viewing geometry. The angle parameters are known for each grid point from the image navigation data. Surface albedo for cloudy cells was estimated from a recent clear scene dataset or a typical value for the local land surface type. UV surface albedo was estimated from a scaling of visible reflectance based on field measurements by McKenzie *et al.* (1996).

If the scene at the point is designated locally cloud-free with no surrounding cloud fraction, then UV spectral flux to the point was calculated from model clear-sky irradiance adjusted for differences between control point and local conditions of estimated surface albedo. Model simulations of variations in spectral irradiance due to surface reflectance have been tabulated to allow these adjustments. Model results for increasing albedo provided an enhancement for UV irradiance caused by multiple scattering between the surface and atmosphere.

Model irradiances were separated into clear-sky direct beam (E_D) and diffuse (E_d) sky components as well as cloudy-sky direct (E_{Dc}) and diffuse (E_{dc}) components, and these were used to determine the total irradiance under overcast, fully clear, or partial cloud cover conditions. When a point location was cloud-free but a non-zero cloud fraction (CF) existed in the $(50\ km)^2$ box centered on that point (CF is calculated from cloud7 cells classified within the surrounding box), the irradiance for that point was modified by increasing the magnitude of downward direct irradiance to account for UV direct beam radiation scattered from cloud sides, and reducing the magnitude of downward diffuse irradiance to represent the cloud-filled fraction of the surrounding sky (see Equation 1). When a point location was covered by cloud, the total irradiance to that point was calculated as the sum of direct UV irradiance transmitted through cloud, the diffuse irradiance from the non-cloudy surrounding sky, and the diffuse irradiance from the cloud-filled sky fraction (Equation 2).

Calculations for total irradiance (E_t) were thus:

for Sun not obscured ;

$$E_t = E_D + E_{dc}\,(CF) + E_d\,(1\text{-}CF), \qquad [1]$$

and for Sun obscured ;

$$E_t = E_{Dc} + E_d\,(1\text{-}CF) + E_{dc}\,(CF). \qquad [2]$$

The resulting UV total irradiances for a given spectral band were mapped into the same projection as the input satellite data. Sampling the output data provided statistics

on the range of UV irradiances within the study area.

Parameters on image pixel type, surface albedo and cloud optical depth retrieved from the procedure described above were used as input to the TUV radiative transfer model (Madronich and Flocke, 1998) to calculate spectral actinic flux and photolysis rates for points within the gridded dataset. These results were used to evaluate the effects of surface reflectance and cloud optical parameters on actinic flux, as well as the differences between point-specific and areal-average photolysis rates derived from the calculated actinic fluxes.

4. RETRIEVAL RESULTS AND PATTERN CHARACTERISTICS

GOES-West satellite digital data were applied to mesoscale mapping of downward UV irradiance for a region of the central Rocky Mountains centered on the Desert Research Institute's Storm Peak Laboratory using the method described in Section 3. The topography of this region (shown in Figure 2) generally is a factor in the spatial variability of surface albedo (due to snow cover distribution) and cloud patterns (orographically-enhanced cloud formation as seen in Figure 3).

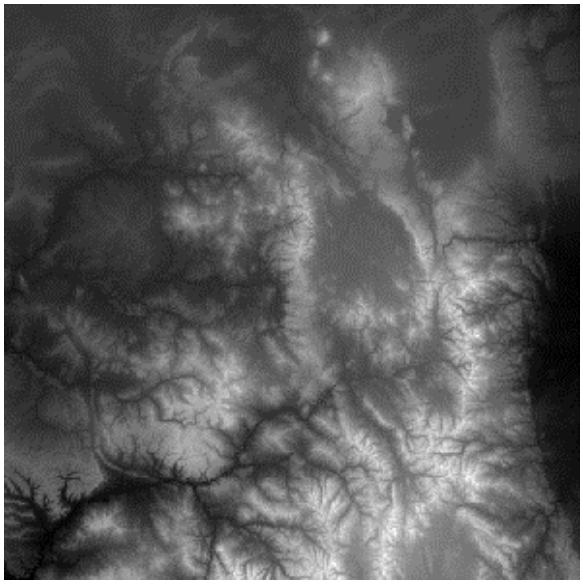

Figure 2. Digital elevation image of study area in the central Rocky Moutains (brighter pixels have higher elevation).

The classification and radiative transfer retrieval methods were applied to image datasets over this region for multiple times and days. Figure 4 portrays the cell classification for the time corresponding to Figure 3. The distinction between water cloud and ice cloud is indicated for areas of orographic convection and portions of the wave cloud areas, and some areas of snow cover are identified as well.

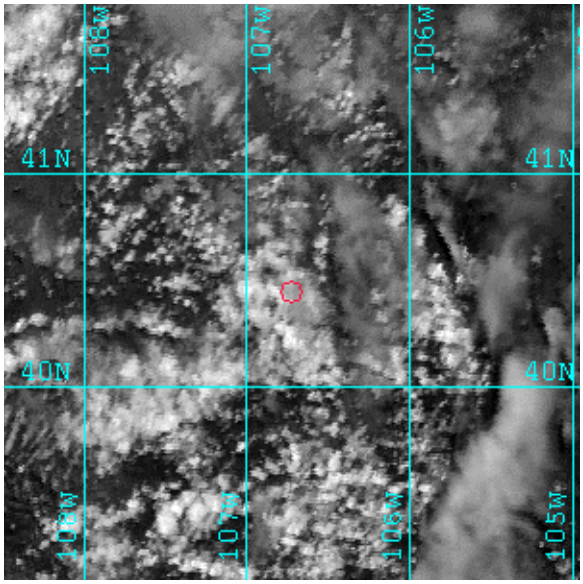

Figure 3. GOES visible image of study region (matching area of Figure 2) in central northern Colorado for 2020 UTC on 9 April 2002, showing bright convective and wave cloud development associated with topography. The red circle indicates the location of the Storm Peak Laboratory monitoring site.

Figure 4. Results of multispectral image classification for 2020 UTC on 9 April 2002 over study region (same geographic area as Figure 3), showing scaled images of pixel types [black=land, dark gray = snow, light gray=ice cloud, white = water cloud].

The UV irradiance field (Figure 5) shows significant mesoscale variability due to the effects of cloud cover, surface albedo, and the presence of surrounding cloud (adjacent pixel effects). The brightest areas are found in clear sky conditions, with maximum values for snow-covered land surfaces under clear sky. The darkest regions correspond to reduced UV irradiance caused by cloud cover, with spots indicating areas of isolated cumulus and smooth gray zones associated with extensive cloud layers.

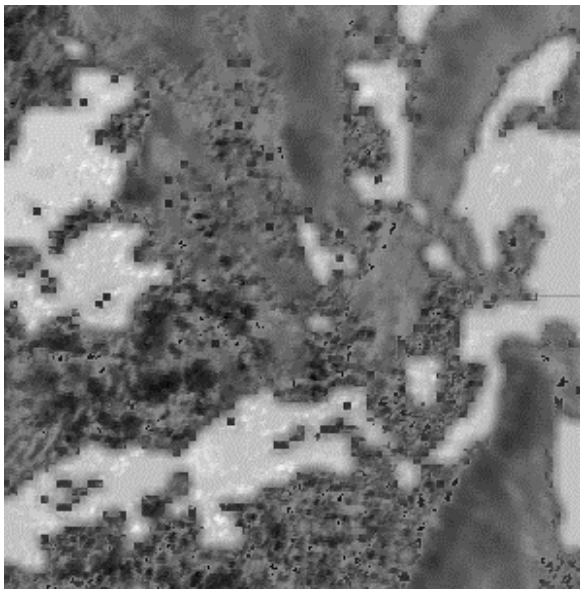

Figure 5. Results of model-based retrieval analysis at 2020 UTC on 9 April 2002 for 317-nm downward surface irradiance (brighter shades indicate larger irradiance values in the cloud-free areas).

Figure 6 indicates that the retrieval procedure provides very good estimates of downwelling irradiance even in the presence of cloud cover, for the 2020 UTC image time of Figure 5 as well as at other times throughout the study day. GOES data are generally available at a 15-minute time resolution, facilitating this type of time-specific comparison with ground measurements and cloud conditions, analysis of time series, and calculation of time-composited parameters such as total daily spectral insolation.

Model calculations of actinic flux and photolysis rates were carried out using the TUV model and the retrieved mesoscale gridded parameters of pixel type, cloud optical depth and surface albedo, for a 100 km x 100 km area centered on the Storm Peak Laboratory site. Figure 7 provides summary information on the range of 305-nm actinic flux values within pixel type categories. Pixels not covered by cloud (land and snow types) show the largest magnitudes of actinic flux, as expected. The largest values of actinic flux are calculated for high albedo surfaces (snow) where cloud is not obscuring the sun. Pixels diagnosed as having ice cloud overhead have the smallest values but also the largest range, indicating the sensitivity to cloud thickness (ranging from thin cirrus to deep, cold cloud layers).

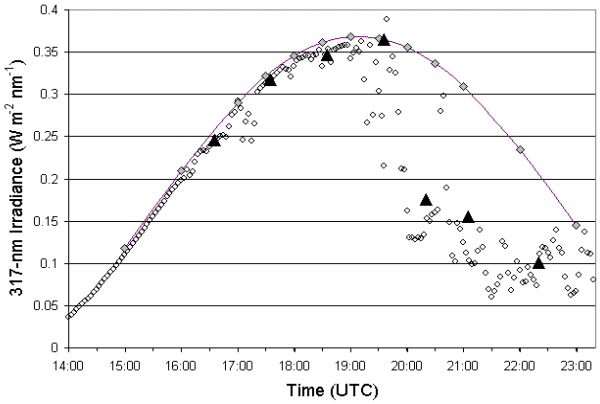

Figure 6. Retrieved estimates (triangles), clear-sky model calculations (smooth curve) and measurements (circles) for 317-nm irradiance on 9 April 2002 at Storm Peak Laboratory.

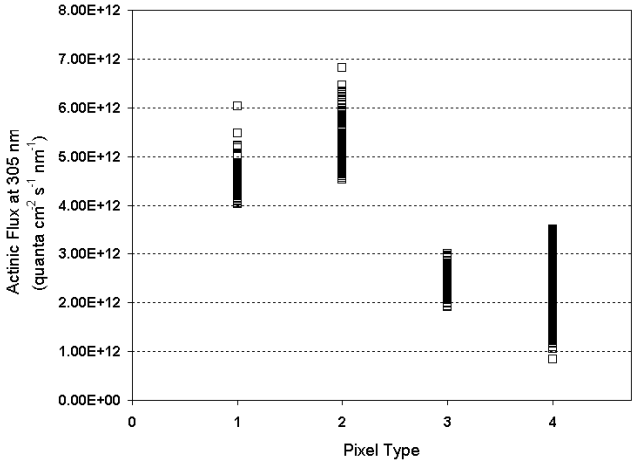

Figure 7. Spectral actinic flux at 305 nm calculated for a 100 km x 100 km area centered on the Storm Peak Laboratory measurement site for 2215 UTC on 9 April 2002, distributed by pixel type (1 = land, 2 = snow, 3 = water cloud, 4 = ice cloud).

Ozone photolysis rates for the 100 km x 100 km analysis area centered on SPL are shown in Figure 8. Note that the photolysis rate values calculated for pixels within this grid vary by a factor of three, indicating the large mesoscale variability in photochemical processes, which can dramatically alter air quality process mechanisms. Also, the calculated photolysis rate at the measurement site (0.013 hr^{-1}) was near the minimum value determined for the entire analysis area, due to cloud cover over the

site itself. Measurements of a point value would in this case have significantly underestimated the photolysis rates for the area. Instead of relying on point measurements of UV irradiance or actinic flux or forward model results based on site-specific model input parameters, a more robust approach for representation of photochemical processes within a geographic area would be the assimilation of available point measurements with the output of gridded parameters derived from the satellite retrieval procedure.

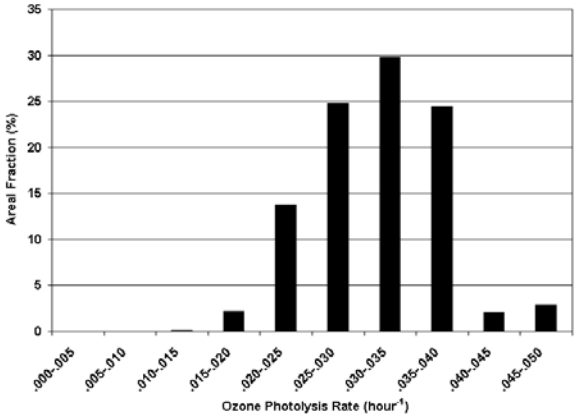

Figure 8. Frequency distribution of ozone photolysis rates calculated for a 100 km x 100 km area centered on the Storm Peak Laboratory measurement site for 2215 UTC on 9 April 2002.

Any mapping procedure that combines radiative transfer modeling with satellite datasets requires decisions regarding the resolution of input parameters such as surface elevation, atmospheric conditions (ozone column amount; aerosol optical depth) and sun-satellite scattering geometry. For this study, we have limited the geographic domain and used domain-average conditions of viewing geometry for rapid processing. Point-specific values of surface albedo and cloud optical depth were retrieved. Surface elevation and ozone column amount variations within the domain where then used to scale the resulting irradiance values according to point-specific variations in surface elevation, ozone column amount and aerosol optical depth for locales of interest.

Comparisons were made for spectral UV irradianc e estimated by this methods at several USDA UVB Network sites within a larger region of Colorado and adjoining states. Locations included the Storm Peak Laboratory (SPL), Table Mountain (TBL), Nunn (NUN) and Lamar (LAM) sites in Colorado as well as a site at Logan (LGN), Utah as shown in the GOES visible image for a mid-day case study from 9 January 2004 (Figure 9). The image classification and UV mapping procedure were applied to the image time, with the result for 317-μm irradiance shown in Figure 10.

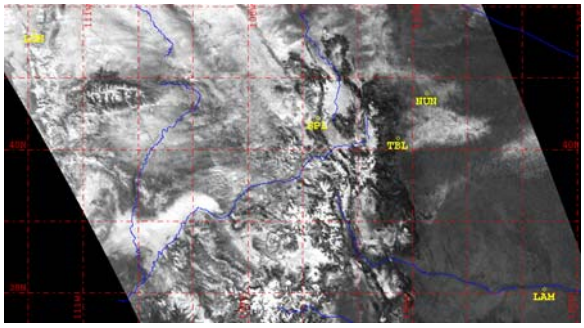

Figure 9. GOES visible satellite image1845 UTC on 9 January 2004 with graphic overlay of rivers (blue), geographic grid (red) and measurement site locations (yellow).

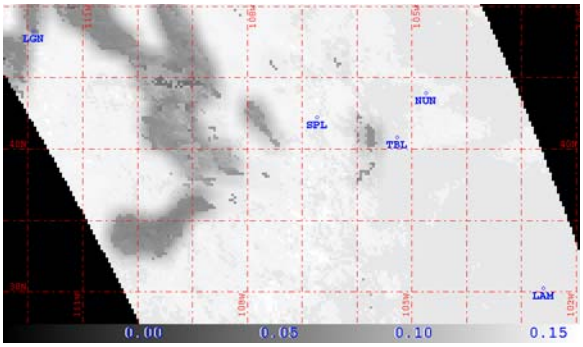

Figure 10. Retrieved estimates of 317-nm downward surface irradiance (W m^{-2} nm^{-1}) corresponding the image time and domain shown in Figure 9. This mapped distribution was used to obtain the point values for measurement sites (blue) listed in Table 1.

Table 1 lists the estimated and measured irradiances for the spatially distributed sampling locations in the study area. The high-elevation site (SPL) was classified as clear in the retrieval procedure, and it has the largest measured and estimated irradiance values in the group as expected. The lower elevation sites had a positive bias in the estimated values, except for LGN which was classified as cloudy and had close agreement between measured and estimated irradiances.

Evaluation of the causes of discrepancies between measured and estimated irradiances is needed. One source of uncertainty is the variation in surface albedo within geographic range of a measurement location, that contributes to the diffuse component of downward irradiance measured at the location. Inaccurate estimates of surface albedo can have a significant impact on mesoscale distribution of UV irradiance and photolysis rates. Figure 11 presents measured downward spectral actinic flux obtained from an actinic (hemispheric incidence) spectroradiometer at Storm Peak Laboratory during the time period shown in Figure 9, along with estimates derived from the TUV radiative transfer model.

for two different values of surface albedo. It is seen that model results which assumed a smaller surface albedo (0.20) more closely match the observations. The surface albedo at the SPL location calculated from on-site spectroradiometer net flux measurements was near 0.80. In contrast, the albedo estimated from the satellite method was lower, due to the mesoscale variability of the mixed snow- and forest-covered terrain in the vicinity of the SPL site (see Figure 9). Thus, additional study of mesoscale albedo effects and other parameters that influence the retrieval method is needed, with application of both GOES data (for high temporal resolution) as well as satellite data sources such as MODIS that can provide higher spatial resolution.

Table 1. Site-specific values of 317-nm downward surface irradiance (W m^{-2} nm^{-1}) measured and estimated for 1850 UTC 9 January 2004 obtained for site locations shown in Figure 9.

Site ID	Elevation (meters)	Measured Irradiance	Estimated Irradiance
LAM	1120	0.088	0.118
LGN	1368	0.076	0.075
NUN	1641	0.093	0.123
TBL	1689	0.094	0.124
SPL	3220	0.145	0.144

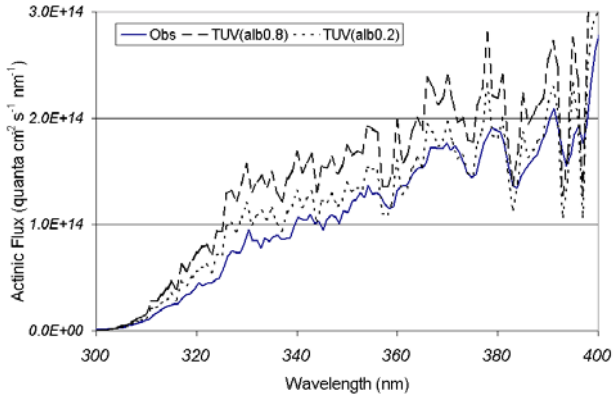

Figure 11. Intercomparison of spectral actinic flux for 19:00 UTC 9 January 2004 at Storm Peak Lab obtained by measurement (solid line), versus model-estimated values for conditions of surface albedo 0.2 (dash-dot line) and surface albedo 0.8 (dotted line).

6. DISCUSSION

A method for mesosale retrieval and mapping of downwelling spectral irradiance has been demonstrated with comparisons to measurements from a mountainous region of Colorado, and this method was also used to map actinic flux and photolysis rates. The results were applied to an evaluation of the correspondence between site-specific measurements and irradiances that might be obtained over a larger area, for example a satellite-derived product with a 100 km grid resolution. UV irradiance climatology at high latitudes and high altitudes is an important aspect of environmental monitoring, where surface albedo is often high even during the summer. Use of high-resolution satellite image data in remote areas can also be applied to improving forecasts of UV exposure (Long et al., 1996) with specific application to agricultural/forest workers, satellite monitoring of actinic flux (Mayer *et al.,* 1998) for analysis of photochemical air pollution processes, verification of larger-scale models for tropospheric photochemistry (Tie *et al*., 2003) , and study of biogenic emissions influenced by absorbed UV and photosynthetically active radiation.

Mesoscale mapping of spectral actinic flux and photolysis is of value to applications such as air quality forecasting, for which NOAA is currently focusing an effort toward prediction of tropospheric ozone concentrations. (Stockwell *et al*., 2002). Since forecasting models typically have difficulty in predicting time series of mesoscale cloud distribution, merging satellite observations and model forecast products offers the most reliable approach to predicting diurnal evolution of ozone in the troposphere.

Acknowledgments

This research was supported by the Desert Research Institute and grants from NOAA, NSF and USDA.

References

Bigelow, D. S., J. R. Slusser, A. F. Beaubien, and J. H. Gibson, "The USDA Ultraviolet Radiation Monitoring Program", *Bull. Amer. Meteor. Soc., 79,* 601-615, 1998.

Caldwell, M.M., L.O. Björn, J. F. Bornman, S.D. Flint, G. Kulandaivelu, A.H. Teramura and M. Tevini, "Effects of increased solar ultraviolet radiation on terrestrial ecosystems, 1998", In: Environmental Effects of Ozone Depletion: 1998 Assessment, United Nations Environment Programme, 205 pp., ISBN 92-807-1724-3 UNEP.

Frederick, J. E., and D. Lubin, "The budget of biologically active ultraviolet radiation in the Earth-Atmosphere system", *J. Geophys. Res.*, *93*, 3825-3832 1988.

Gao, W., J. Slusser, J. Gibson, G. Scott, D. Bigelow, J. Kerr, and B. McArthur, "Direct-Sun column ozone retrieval by the ultraviolet multifilter rotating shadowband radiometer and comparison with those from Brewer and

Dobson spectrophotometers", *Appl. Opt. 40,* 3149-3155, 2001.

Gröbner, J., and J. Kerr, "Ground-based determination of the spectral ultraviolet extraterrestrial solar irradiance: Providing a link between space-based and ground-based solar UV measurements", *J. Geophys. Res., 106*, 7211-7217, 2001.

Harrison, L., and J. Michalsky, "Objective algorithms for the retrieval of optical depths from ground-based measurements", *Appl. Opt., 33,* 5126-5132, 1994.

Herman, J. R., N. Krotkov, E. Celarier, D. Larko, and G. Labow, " The distribution of UV radiation at the Earth's surface from TOMS measured UV-backscattered radiances", *J. Geophys. Res.*, *104***,** 12,059-12,076, 1999.

Kneizys, F.X., E.P. Shettle, W.O. Gallery, J.H. Chetwynd, L.W., Abreu, J.E.A. Selby, S.A. Clough and R.W. Fenn, "Atmospheric transmittance/radiance: computer code LOWTRAN 6", Air Force Geophysics Laboratroy, Report AFGL-TR-83-0187, Hanscom AFB MA. 1983.

Long, C.S., A.J. Miller, H.T.Lee, J.D.Wild, R.C.Przywarty, and D. Hufford, "Ultraviolet Index forecasts issued by the National Weather Service," *Bull. Amer. Meteor. Soc*., *77*, 729-747, 1996.

Madronich, S., "Implications of recent total atmospheric ozone measurements for biologically active ultraviolet radiation reaching the Earth's surface," *Geophys. Res. Lett*., *19*, 37-40, 1992.

Madronich, S., and C. Granier, "Impact of recent total ozone changes on tropospheric ozone photodissociation, hydrocyl radicals, and methane trends," *Geophys. Res. Lett*., *19*, 465- 467, 1992.

Madronich, S. and S. Flocke, The role of solar radiation in atmospheric chemistry, in Handbook of Environmental Chemistry (P. Boule, ed.), Springer-Verlag, Heidelberg, pp. 1-26, 1998.

Mayer, B., C.A. Fischer, and S. Madronich, "Estimation of surface actinic flux from satellite (TOMS) ozone and cloud reflectivity measurements," *Geophys. Res. Letts.*, *25*, 4321-4324, 1998.

McKenzie, R. L., M. Kotkamp, W. Ireland, "Upwelling UV spectral irradiances and surface albedo measurements at Lauder, New Zealand", *Geophys. Res. Letts., 23*, 1757-1760, 1996.

Meerkötter, R., B. Wissinger, and G. Seckmeyer, "Surface UV from ERS2/GOME and NOAA/AVHRR data: A case study", *Geophys. Res. Lett., 24*, 1939-1942, 1997.

Molina, L.T., and M.J. Molina, "Absolute absorption cross sections of ozone in the 185-350 nm wavelength range, *J. Geophys. Res., 91*, 14501-14509, 1986.

Ricchiazzi, P., S.Yang, C. Gautier, and D. Sowle, "SBDART: A research and teaching software tool for plane-parallel radiative transfer in the Earth's atmosphere", *Bull., Amer. Meteor., Soc.*, *79*, 2101-2114, 1998.

Stockwell, W.R., R.S. Artz, J.F. Meagher, R.A. Petersen, K.L. Schere, G.A. Grell, S.E. Peckham, A.F. Stein, R.V. Pierce, J.M. O'Sullivan, and P.-Y. Whung, "The Scientific Basis of NOAA's Air Quality Forecasting Program", *EM, December 20-27*, 2002.

Tie, X., S. Madronich, S. Walters, R. Zhang, P. Rasch, and W. Collins, "Effect of clouds on photolysis and oxidants in the troposphere", *J. Geophys. Res., 108,* 8545, doi: 10.1029/2003JD003659, 2003.

Turner, J., G.J. Marshall, and R.S. Ladkin, "An operational, real-time cloud detection scheme for use in the Antarctic based on AVHRR data", *Int. J. Rem. Sens*., *22*, 3027-3046, 2001.

Verdebout, J., "A method to generate surface UV radiation maps over Europe using GOME, Meteosat, and ancillary geophysical data", *J. Geophys. Res*., *105*, 5049-5058, 2000.

Williams, G., and A. Green, "A cumulative-exposure model for predicting the increase in non-melanoma skin cancer associated with ozone depletion", *Cancer Forum*, *20*, 195-198, 1996.